Basic Interferometry and Optical Testing

- Two Beam Interference
- Fizeau Interferometer
- Twyman-Green Interferometer
- Laser Based Fizeau
- Mach-Zehnder Interferometer
- Typical Interferograms
- Interferograms and Moiré Patterns
- Classical techniques for inputting data into computer

Two-Beam Interference Fringes

$$I = I_1 + I_2 + 2\sqrt{I_1 I_2}\cos(\alpha_1 - \alpha_2)$$

$\alpha_1 - \alpha_2$ is the phase difference between the two interfering beams

$$\alpha_1 - \alpha_2 = \left(\frac{2\pi}{\lambda}\right)(\text{optical path difference})$$

Sinusoidal Interference Fringes

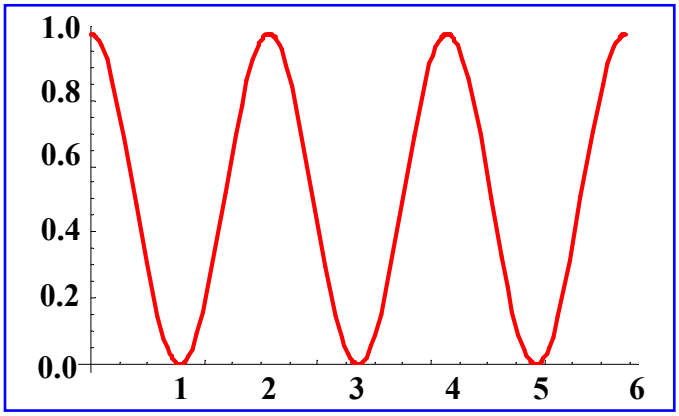

$$I = I_1 + I_2 + 2\sqrt{I_1 I_2}\cos(\alpha_1 - \alpha_2)$$

Classical Fizeau Interferometer

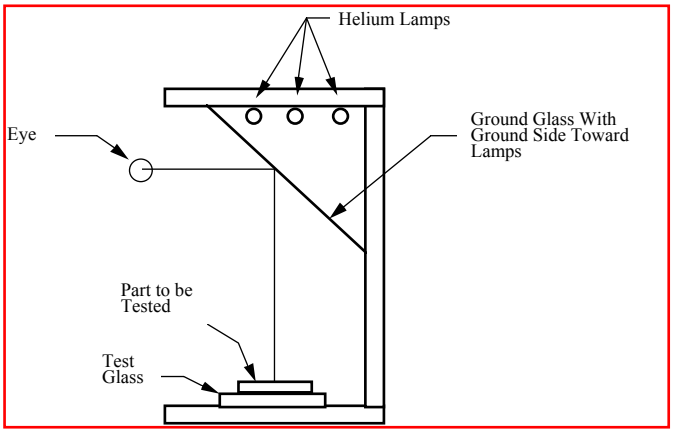

Typical Interferogram Obtained using Fizeau Interferometer

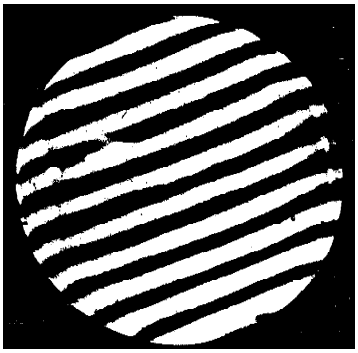

Relationship between Surface Height Error and Fringe Deviation

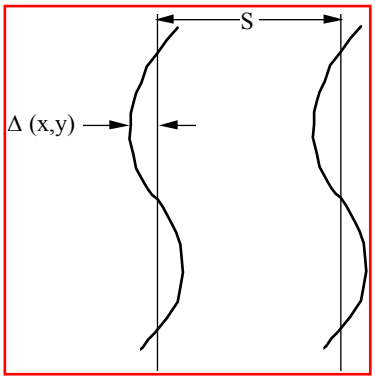

Surface height error = $\left(\frac{\lambda}{2}\right)\left(\frac{\Delta}{S}\right)$

Fizeau Fringes

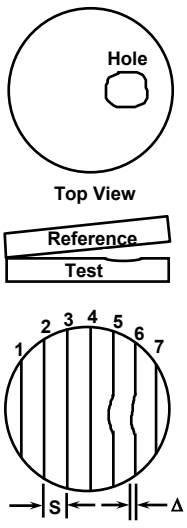

For a given fringe the separation between the two surfaces is a constant.

Height error = (λ/2)(Δ/S)

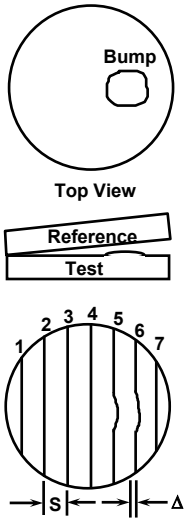

Fizeau Fringes for Concave and Convex Surfaces

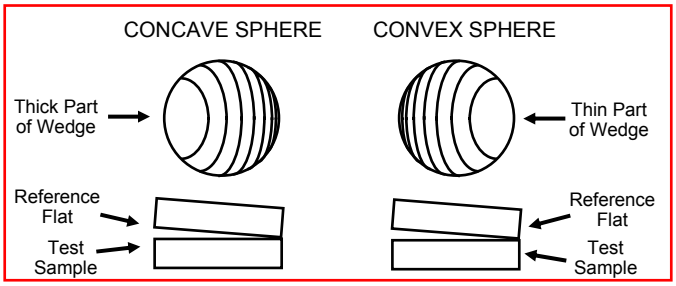

Twyman-Green Interferometer (Flat Surfaces)

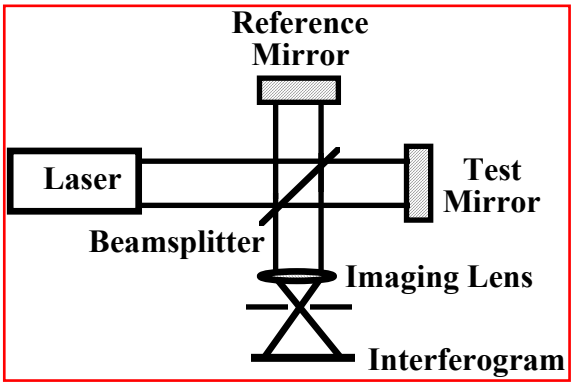

Twyman-Green Interferometer (Spherical Surfaces)

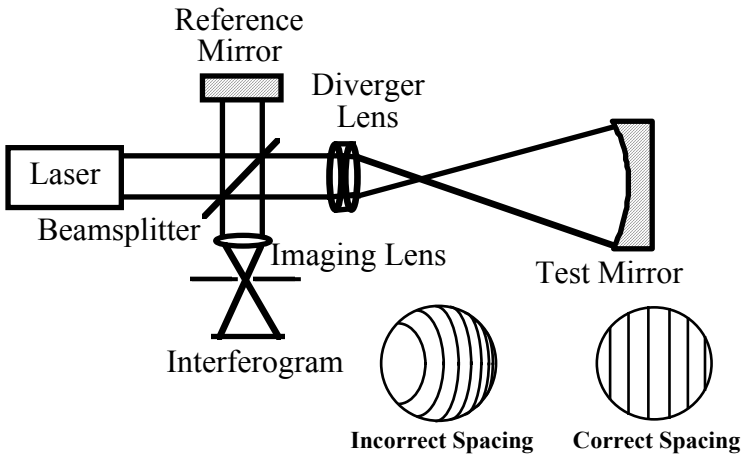

Typical Interferogram

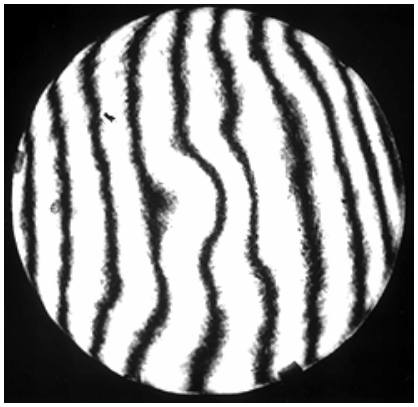

Fizeau Interferometer-Laser Source (Flat Surfaces)

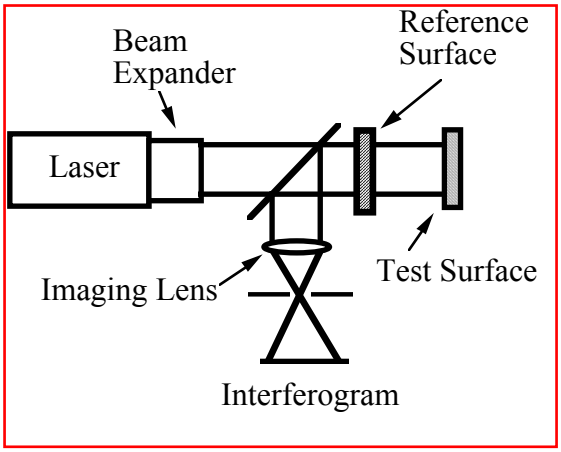

Fizeau Interferometer-Laser Source (Spherical Surfaces)

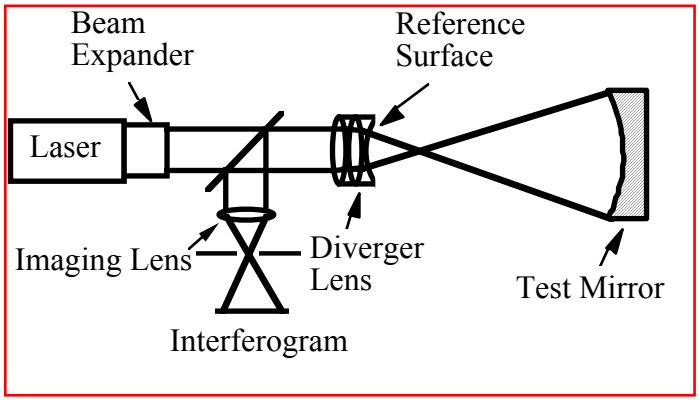

Testing High Reflectivity Surfaces

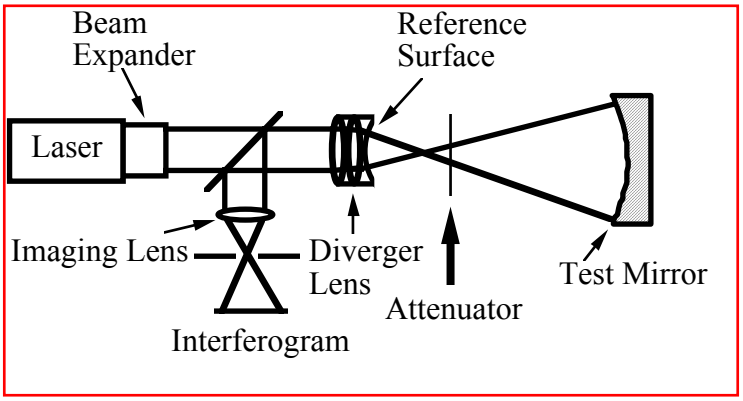

Mach-Zehnder Interferometer

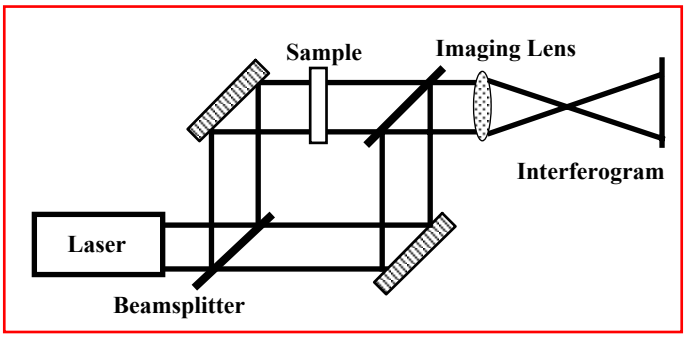

Testing samples in transmission

Laser Beam Wavefront Measurement

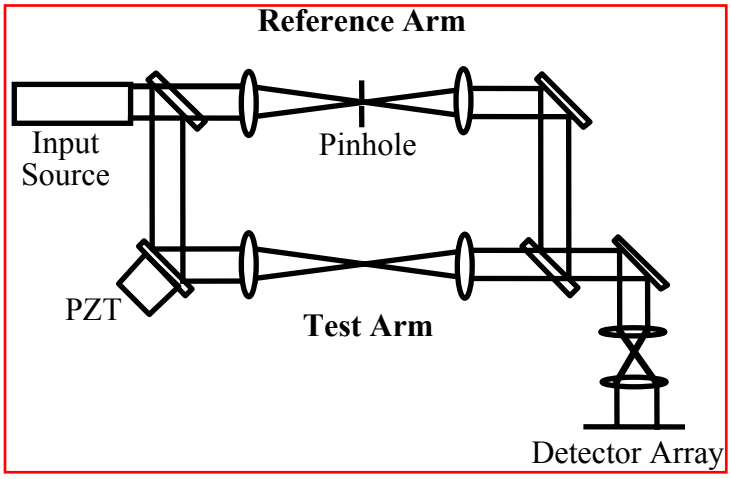

Interferograms, Spherical Aberration

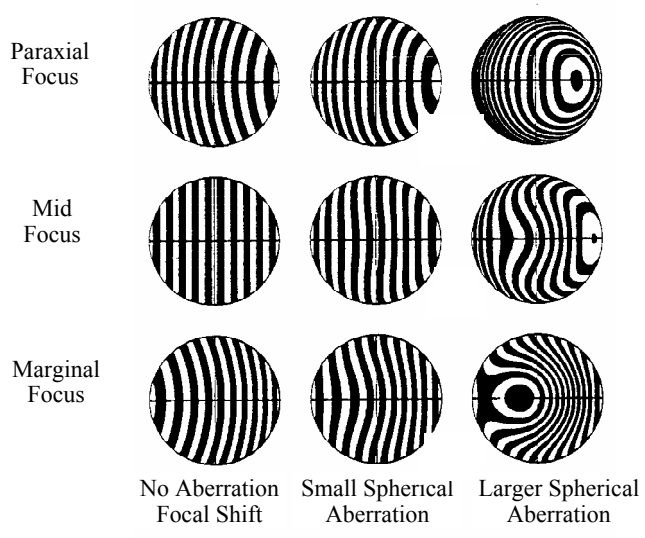

Interferograms
Small Astigmatism, Sagittal Focus

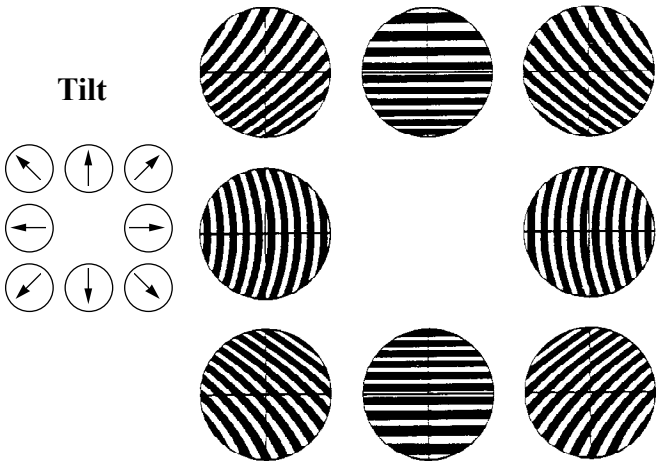

Interferograms
Small Astigmatism, Medial Focus

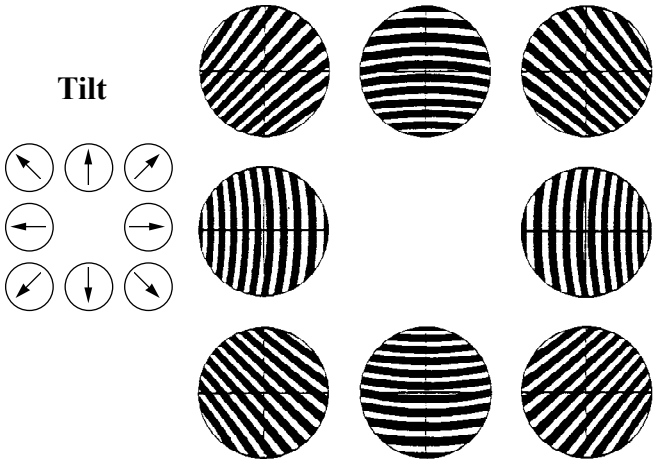

Interferograms, Large Astigmatism, Sagittal Focus, Small Tilt

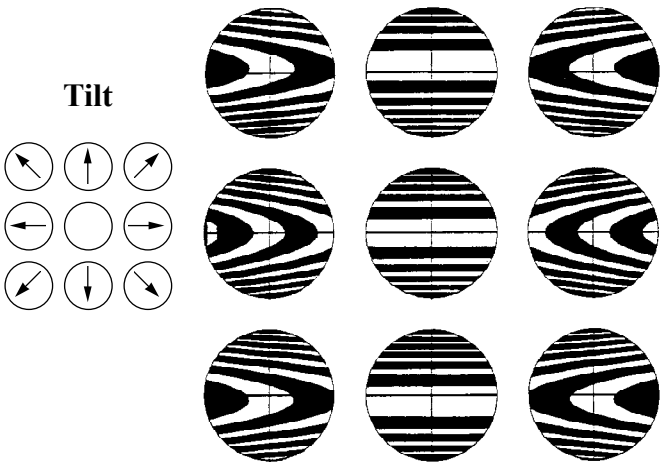

Interferograms, Large Astigmatism, Medial Focus, Small Tilt

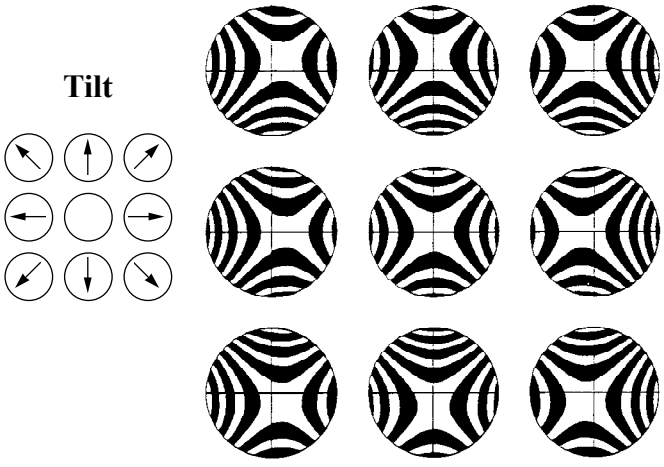

Interferograms Small Coma, Large Tilt

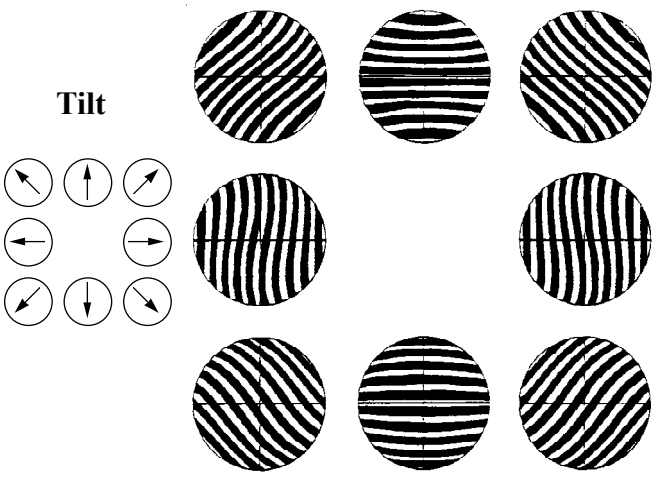

Interferograms
Large Coma, Small Tilt

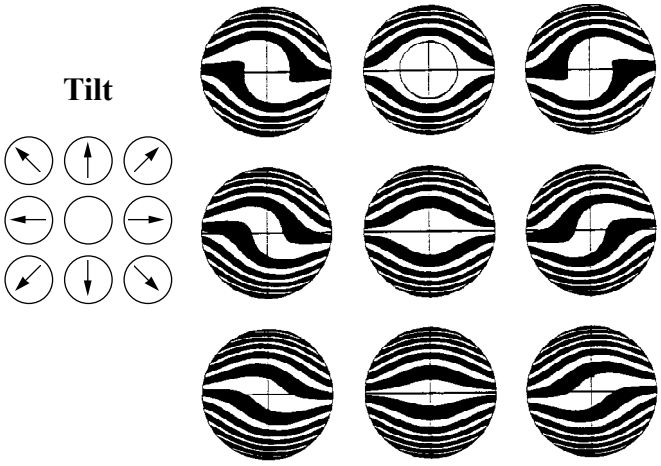

Interferograms
Large Coma, Large Tilt

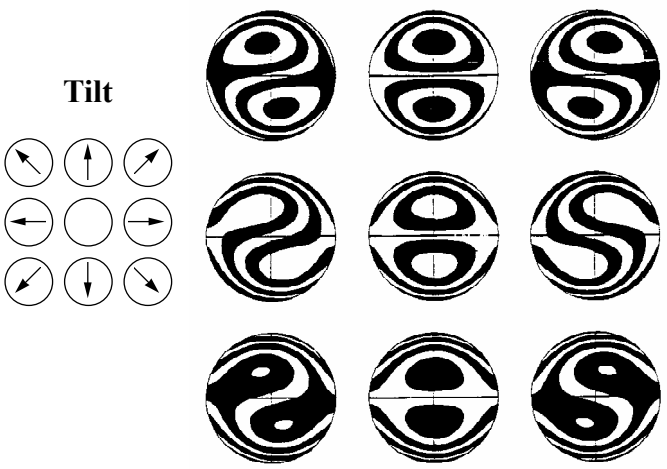

Interferograms
Small Focal Shift

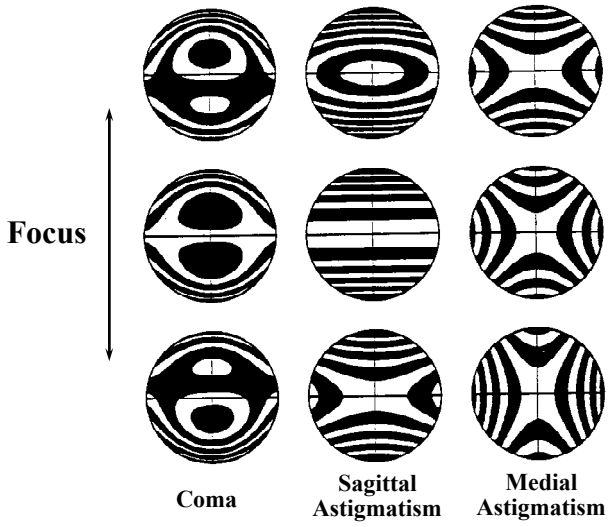

Interferograms
Combined Aberrations

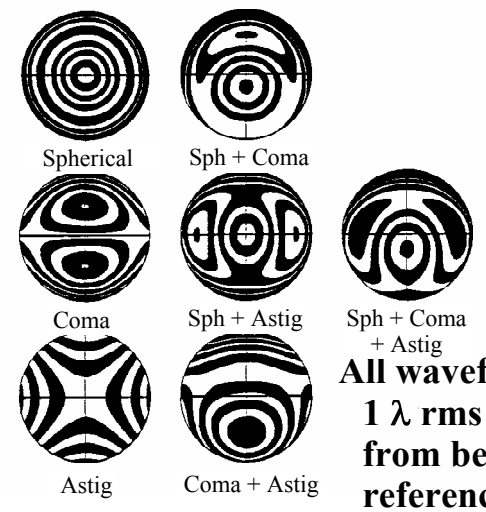

All wavefronts have 1 λ rms departure from best-fitting reference sphere.

16.2. WHAT IS MOIRÉ?

Moiré patterns are extremely useful to help understand basic interferometry and interferometric test results. Figure 16.1 shows the moiré pattern (or beat pattern) produced by two identical straight-line gratings rotated by a small angle relative to each other. A dark fringe is produced where the dark lines are out of step one-half period, and a bright fringe is produced where the dark lines for one grating fall on top of the corresponding dark lines for the second grating. If the angle between the two gratings is increased, the separation between the bright and dark fringes decreases. [A simple explanation of moiré is given by Oster and Nishijima (1963).]

If the gratings are not identical straight-line gratings, the moiré pattern (bright and dark fringes) will not be straight equi-spaced fringes. The following anal-

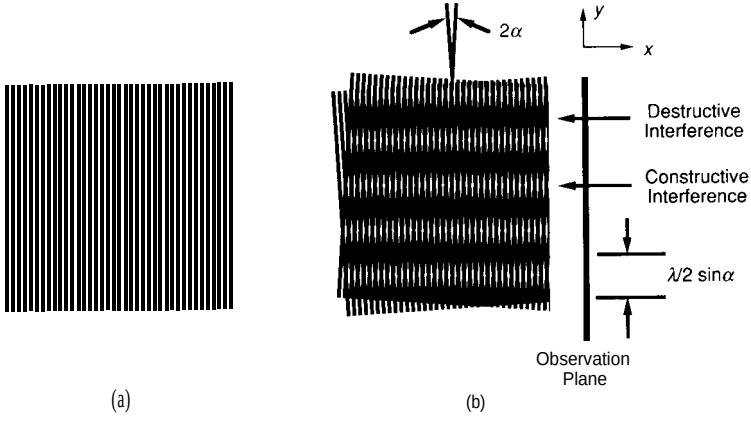

Figure 16.1. (a) Straight-line grating. (b) Moiré between two straight-line gratings of the same pitch at an angle α with respect to one another.

ysis shows how to calculate the moire pattern for arbitrary gratings. Let the intensity transmission function for two gratings $f_1(x, y)$ and $f_2(x, y)$ be given by

$$f_1(x, y) = a_1 + \sum_{n=1}^{\infty} b_{1n} \cos [n\phi_1(x, y)],$$

$$f_2(x, y) = a_2 + \sum_{m=1}^{\infty} b_{2m} \cos [m\phi_2(x, y)], \tag{16.1}$$

where ϕ (x, y) is the function describing the basic shape of the grating lines. For the fundamental frequency, ϕ (x, y) is equal to an integer times 2 π at the center of each bright line and is equal to an integer plus one-half times 2 π at the center of each dark line. The b coefficients determine the profile of the grating lines (i.e., square wave, triangular, sinusoidal, etc.) For a sinusoidal line profile, b_{i1} is the only nonzero term.

When these two gratings are superimposed, the resulting intensity transmission function is given by the product

$$\begin{aligned} f_1(x, y) f_2(x, y) = a_1 a_2 &+ a_1 \sum_{m=1}^{\infty} b_{2m} \cos [m\phi_2(x, y)] \\ &+ a_2 \sum_{n=1}^{\infty} b_{1n} \cos [n\phi_1(x, y)] \\ &+ \sum_{m=1}^{\infty} \sum_{n=1}^{\infty} b_{1n} b_{2m} \cos [n\phi_1(x, y)] \cos [m\phi_2(x, y)]. \end{aligned} \tag{16.2}$$

The first three terms of Eq. (16.2) provide information that can be determined by looking at the two patterns separately. The last term is the interesting one, and can be rewritten as

$$\begin{aligned} \text{Term 4} = &\tfrac{1}{2} b_{11} b_{21} \cos [\phi_1(x, y) - \phi_2(x, y)] \\ &+ \tfrac{1}{2} \sum_{m=1}^{\infty} \sum_{n=1}^{\infty} b_{1n} b_{2m} \cos [n\phi_1(x, y) - m\phi_2(x, y)]; \\ &\quad \text{n and } m \text{ both } \# 1 \\ &+ \tfrac{1}{2} \sum_{m=1}^{\infty} \sum_{n=1}^{\infty} b_{1n} b_{2m} \cos [n\phi_1(x, y) + m\phi_2(x, y)]x. \end{aligned} \tag{16.3}$$

This expression shows that by superimposing the two gratings, the sum and difference between the two gratings is obtained. The first term of Eq. (16.3)

represents the difference between the fundamental pattern masking up the two gratings. It can be used to predict the moiré pattern shown in Fig. 16.1. Assuming that two gratings are oriented with an angle 2α between them with the y axis of the coordinate system bisecting this angle, the two grating functions $\phi_1(x, y)$ and $\phi_2(x, y)$ can be written as

$$\phi_1(x, y) = \frac{2\pi}{\lambda_1}(x \cos \alpha + y \sin \alpha)$$

and

$$\phi_2(x, y) = \frac{2\pi}{\lambda_2}(x \cos \alpha - y \sin \alpha), \tag{16.4}$$

where λ_1 and λ_2 are the line spacings of the two gratings. Equation (16.4) can be rewritten as

$$\phi_1(x, y) - \phi_2(x, y) = \frac{2\pi}{\lambda_{\text{beat}}} x \cos \alpha + \frac{4\pi}{\bar{\lambda}} y \sin \alpha, \tag{16.5}$$

where $\bar{\lambda}$ is the average line spacing, and λ_{beat} is the beat wavelength between the two gratings given by

$$\lambda_{\text{beat}} = \frac{\lambda_1 \lambda_2}{\lambda_2 - \lambda_1}. \tag{16.6}$$

Note that this beat wavelength equation is the same as that obtained for two-wavelength interferometry as shown in Chapter 15. Using Eq. (16.3), the moiré or beat will be lines whose centers satisfy the equation

$$\phi_1(x, y) - \phi_2(x, y) = M2\pi. \tag{16.7}$$

Three separate cases for moiré fringes can be considered. When $\lambda_1 = \lambda_2 = \lambda$, the first term of Eq. (16.5) is zero, and the fringe centers are given by

$$M\lambda = 2y \sin \alpha, \tag{16.8}$$

where M is an integer corresponding to the fringe order. As was expected, Eq. (16.8) is the equation of equi-spaced horizontal lines as seen in Fig. 16.1. The other simple case occurs when the gratings are parallel to each other with $\alpha = 0$. This makes the second term of Eq. (16.5) vanish. The moiré will then be lines that satisfy

$$M\lambda_{\text{beat}} = x. \tag{16.9}$$

16.3. MOIRÉ AND INTERFEROGRAMS

Now that we have covered the basic mathematics of moiré patterns, let us see how moiré patterns are related to interferometry. The single grating shown in Fig. 16.1 can be thought of as a "snapshot" of a plane wave traveling to the right, where the distance between the grating lines is equal to the wavelength of light. The straight lines represent the intersection of a plane of constant phase with the plane of the figure. Superimposing the two sets of grating lines in Fig. 16.1 can be thought of as superimposing two plane waves with an angle of 2α between their directions of propagation. Where the two waves are in phase, bright fringes result (constructive interference), and where they are out of phase,

dark fringes result (destructive interference). For a plane wave, the "grating" lines are really planes perpendicular to the plane of the figure and the dark and bright fringes are also planes perpendicular to the plane of the figure. If the plane waves are traveling to the right, these fringes would be observed by placing a screen perpendicular to the plane of the figure and to the right of the grating lines as shown in Fig. 16.1. The spacing of the interference fringes on the screen is given by Eqn. (16.8), where λ is now the wavelength of light. Thus, the moiré of two straight-line gratings correctly predicts the centers of the interference fringes produced by interfering two plane waves. Since the gratings used to produce the moiré pattern are binary gratings, the moiré does not correctly predict the sinusoidal intensity profile of the interference fringes. (If both gratings had sinusoidal intensity profiles, the resulting moiré would still not have a sinusoidal intensity profile because of higher-order terms.)

More complicated gratings, such as circular gratings, can also be investigated. Figure 16.4b shows the superposition of two circular line gratings. This pattern indicates the fringe positions obtained by interfering two spherical wavefronts. The centers of the two circular line gratings can be considered the source locations for two spherical waves. Just as for two plane waves, the spacing between the grating lines is equal to the wavelength of light. When the two patterns are in phase, bright fringes are produced; and when the patterns are completely out of phase, dark fringes result. For a point on a given fringe, the difference in the distances from the two source points and the fringe point is a constant. Hence, the fringes are hyperboloids. Due to symmetry, the fringes seen on observation plane *A* of Fig. 16.4b must be circular. (Plane *A* is along the top of Fig. 16.4b and perpendicular to the line connecting the two sources as well as perpendicular to the page.) Figure 16.4c shows a binary representation of these interference fringes and represents the interference pattern obtained by interfering a nontilted plane wave and a spherical wave. (A plane wave can be thought of as a spherical wave with an infinite radius of curvature.) Figure 16.4d shows that the interference fringes in plane B are essentially straight equi-spaced fringes. (These fringes are still hyperbolas, but in the limit of large distances, they are essentially straight lines. Plane *B* is along the side of Fig. 16.4b and parallel to the line connecting the two sources as well as perpendicular to the page.)

The lines of constant phase in plane *B* for a single spherical wave are shown in Fig. 16.5a. (To first-order, the lines of constant phase in plane *B* are the same shape as the interference fringes in plane *A.)* The pattern shown in Fig. 16.5a is commonly called a zone plate. Figure 16.5b shows the superposition of two linearly displaced zone plates. The resulting moiré pattern of straight equi-spaced fittings illustrates the interference fringes in plane *B* shown in Fig. 16.4b.

Superimposing two interferograms and looking at the moiré or beat produced can be extremely useful. The moiré formed by superimposing two different

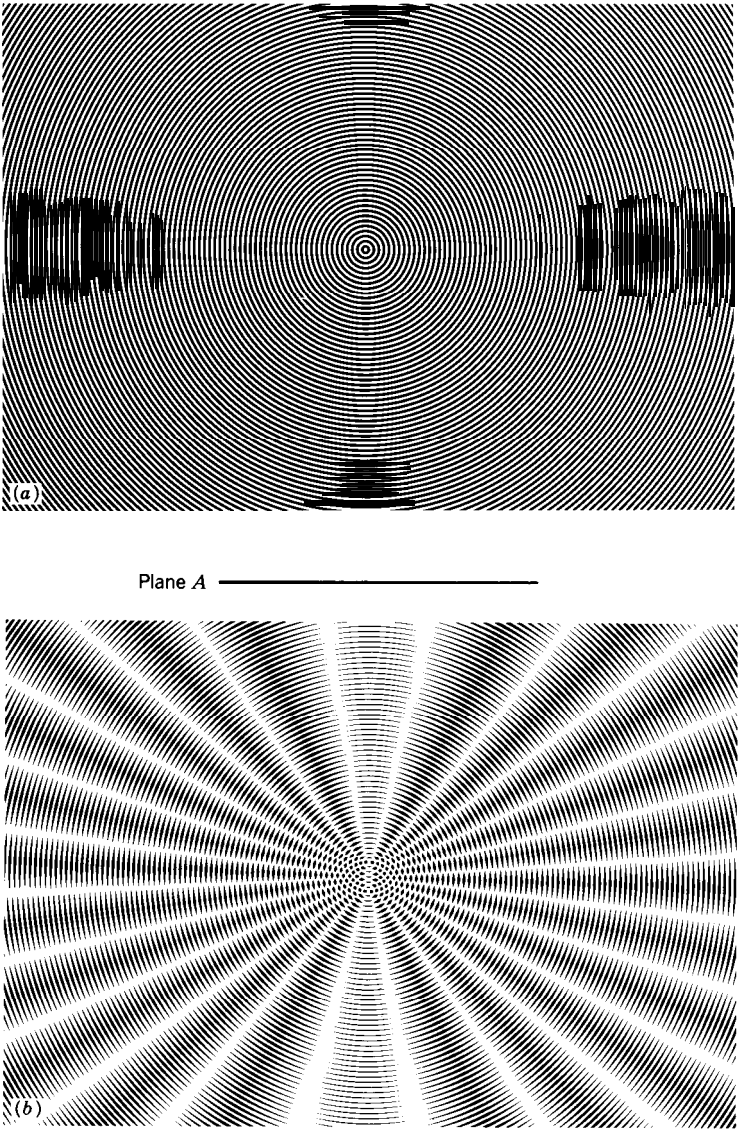

Figure 16.4. Interference of two spherical waves. (a) Circular line grating representing a spherical wavefront. ***(b)*** Moiré pattern obtained by superimposing two circular line patterns. (c) Fringes observed in plane ***A.*** (d) Fringes observed in plane B.

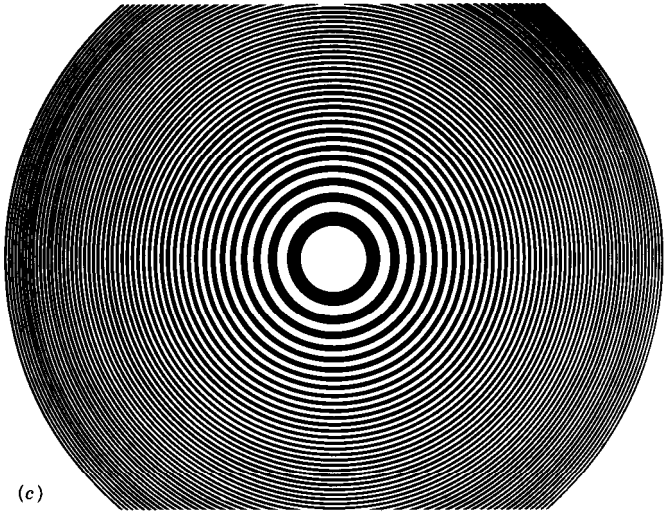

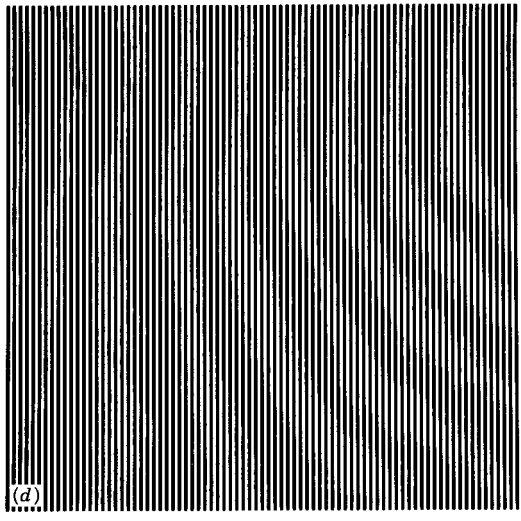

Figure 16.4. (Continued)

interferograms shows the difference in the aberrations of the two interferograms. For example, Fig. 16.6 shows the moiré produced by superimposing two computer-generated interferograms. One interferogram has 50 waves of tilt across the radius (Fig. 16.6a), while the second interferogram has 50 waves of tilt plus 4 waves of defocus (Fig. 16.6b). If the interferograms are aligned such that the tilt direction is the same for both interferograms, the tilt will cancel and

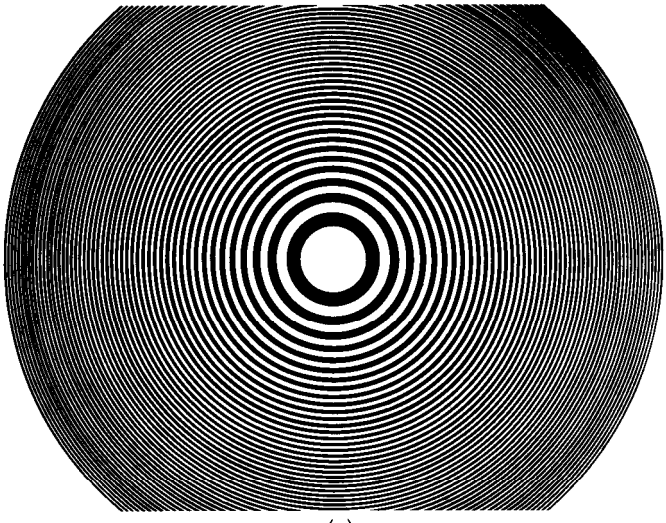

(a)

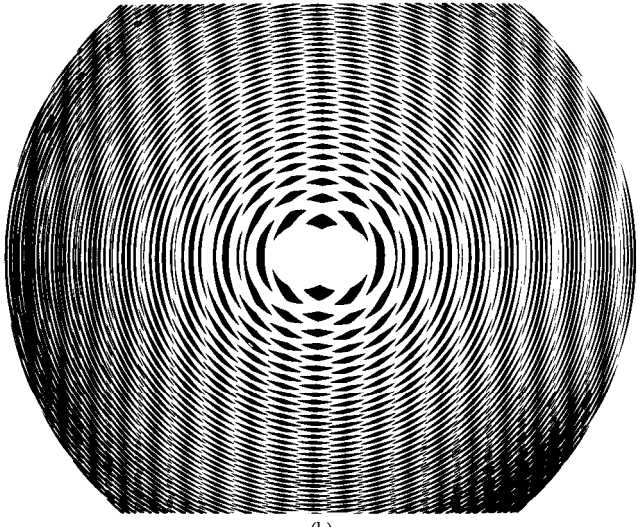

(b)

Figure 16.5. Moiré pattern produced by two zone plates. (a) Zone plate. (b) Straight-line fringes resulting from superposition of two zone plates.

only the 4 waves of defocus remain (Fig. 16.6c). In Fig. 16.6d, the two interferograms are rotated slightly with respect to each other so that the tilt will not quite cancel. These results can be described mathematically by looking at the two grating functions:

$$\phi_1(x, y) = 2\pi(50\rho \cos \phi + 4\rho^2)$$

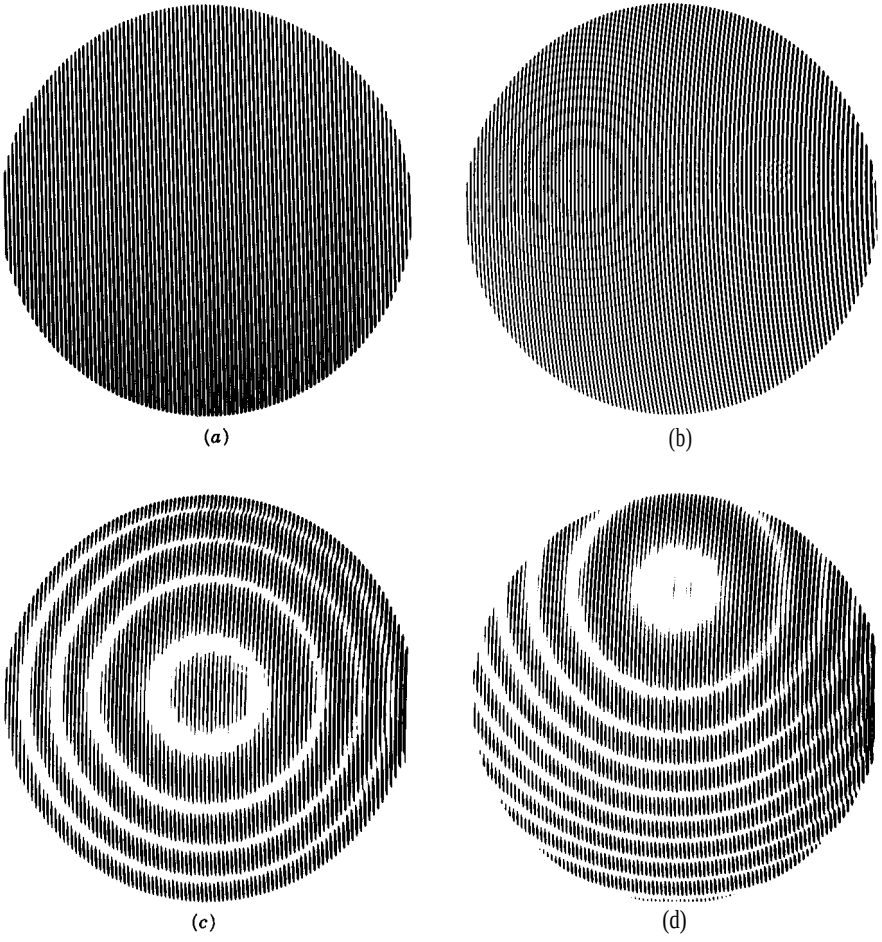

Figure 16.6. Moiré between two interferograms. (a) Interferogram having 50 waves tilt. (6) Interferogram having 50 waves tilt plus 4 waves of defocus. (c) Superposition of (a) and (b) with no tilt between patterns. (d) Slight tilt between patterns.

and

$$\phi_2(x, y) = 2\pi[50\rho \cos(\phi + \alpha)]. \tag{16.16}$$

A bright fringe is obtained when

$$50\rho[\cos\phi - \cos(\phi + \alpha)] + 4\rho^2 = M. \tag{16.17}$$

If $\alpha = 0$, the tilt cancels completely and four waves of defocus remain; otherwise, some tilt remains in the moiré pattern.

Figure 16.7 shows similar results for interferograms containing third-order aberrations. Spherical aberration with defocus and tilt is shown in Fig. 16.7d. One interferogram has 50 waves of tilt (Fig. 16.6a), and the other has 55 waves tilt, 6 waves third-order spherical aberration, and -3 waves defocus (Fig. 16.7a). Figure 16.7e shows the moiré between an interferogram having 50 waves of tilt (Fig. 16.6a) with an interferogram having 50 waves of tilt and 5 waves of coma (Fig. 16.7b) with a slight rotation between the two patterns. The moiré between an interferogram having 50 waves of tilt (Fig. 16.6a) and one having 50 waves of tilt, 7 waves third-order astigmatism, and -3.5 waves defocus (Fig. 16.7c) is shown in Fig. 16.7f. Thus, it is possible to produce simple fringe patterns using moiré. These patterns can be photocopied onto transparencies and used as a learning aid to understand interferograms obtained from third-order aberrations.

A computer-generated interferogram having 55 waves of tilt across the radius, 6 waves of spherical and -3 waves of defocus is shown in Fig. 16.7a. Figure 16.8a shows two identical interferograms superimposed with a small rotation between them. As expected, the moiré pattern consists of nearly straight equi-spaced lines. When one of the two interferograms is slipped over, the resultant moiré is shown in Fig. 16.8b. The fringe deviation from straightness in one interferogram is to the right and, in the other, to the left. Thus the sign of the defocus and spherical aberration for the two interferograms is opposite, and the moiré pattern has twice the defocus and spherical of each of the individual interferograms. When two identical interferograms given by Fig. 16.7a are superimposed with a displacement from one another, a shearing interferogram is obtained. Figure 16.9 shows vertical and horizontal displacements with and without a rotation between the two interferograms. The rotations indicate the addition of tilt to the interferograms. These types of moiré patterns are very useful for understanding lateral shearing interferograms.

Moiré patterns are produced by multiplying two intensity-distribution functions. Adding two intensity functions does not give the difference term obtained in Eq. (16.3). A moiré pattern is not obtained if two intensity functions are added. The only way to get a moiré pattern by adding two intensity functions is to use a nonlinear detector. For the detection of an intensity distribution given by $I_1 + I_2$, a nonlinear response can be written as

$$\text{Response} = a(I_1 + I_2) + b(I_1 + I_2)^2 + \cdots. \tag{16.18}$$

This produces terms proportional to the product of the two intensity distributions in the output signal. Hence, a moiré pattern is obtained if the two individual intensity patterns are simultaneously observed by a nonlinear detector (even if they are not multiplied before detection). If the detector produces an output linearly proportional to the incoming intensity distribution, the two intensity patterns must be multiplied to produce the moiré pattern. Since the eye

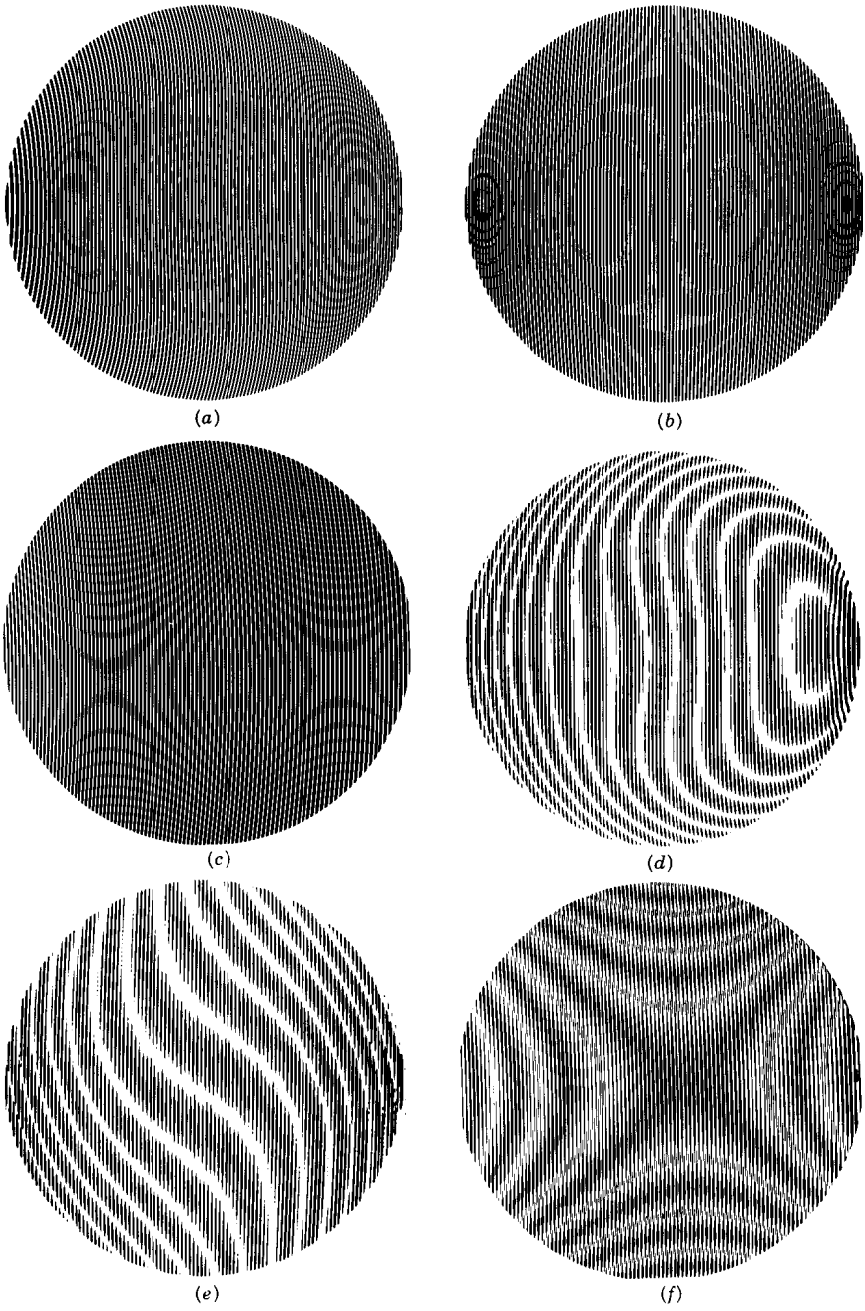

Figure 16.7. Moiré patterns showing third-order aberrations. Interferograms containing (*a*) 55 waves tilt, 6 waves of third-order spherical aberration, and −3 waves of defocus, (*b*) 50 waves tilt and 5 waves coma, and (*c*) 50 waves tilt, 7 waves astigmatism, and −3.5 waves of defocus. (*d*) Moiré pattern between Fig. 16.6*a* and 16.7*a*. (*e*) Moiré pattern between Fig. 16.6*a* and 16.7*b*. (*f*) Moiré pattern between Fig. 16.6*a* and 16.7*c*.

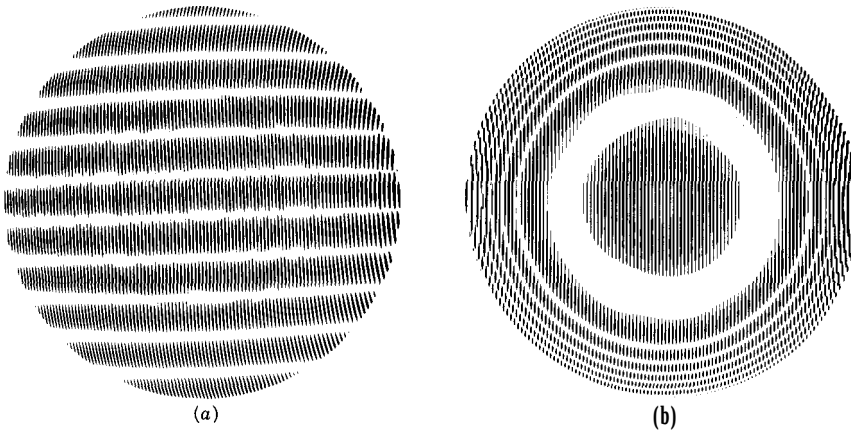

Figure 16.8. Moire pattern by superimposing two identical interferograms (from Fig. 16.7a). (a) Both patterns having the same orientation. (b) With one pattern flipped.

is a nonlinear detector, moiré can be seen whether the patterns are added or multiplied. A good TV camera, on the other hand, will not see moiré unless the patterns are multiplied.

16.4. HISTORICAL REVIEW

Since Lord Rayleigh first noticed the phenomena of moiré fringes, moiré techniques have been used for a number of testing applications. Righi (1887) first noticed that the relative displacement of two gratings could be determined by observing the movement of the moiré fringes. The next significant advance in the use of moiré was presented by Weller and Shepherd (1948). They used moiré to measure the deformation of an object under applied stress by looking at the differences in a grating pattern before and after the applied stress. They were the first to use shadow moiré, where a grating is placed in front of a nonflat surface to determine the shape of the object behind it by using the shape of the moiré fringes. A rigorous theory of moiré fringes did not exist until the mid-fifties when Ligtenberg (1955) and Guild (1956, 1960) explained moiré for stress analysis by mapping slope contours and displacement measurement, respectively. Excellent historical reviews of the early work in moiré have been presented by Theocaris (1962, 1966). Books on this subject have been written by Guild (1956, 1960), Theocaris (1969), and Durelli and Parks (1970). Projection moiré techniques were introduced by Brooks and Helfinger (1969) for optical gauging and deformation measurement. Until 1970, advances in moiré techniques were primarily in stress analysis. Some of the first uses of moiré to measure surface topography were reported by Meadows *et al.* (1970), Takasaki

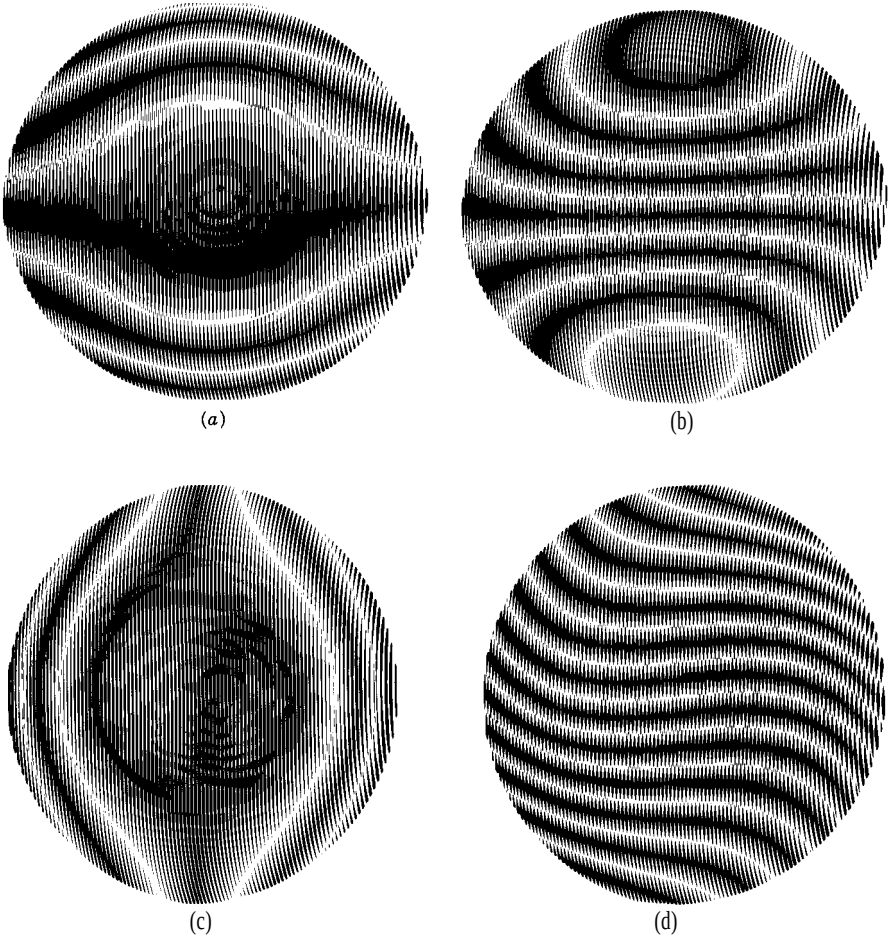

Figure 16.9. Moiré patterns formed using two identical interferograms (from Fig. 16.7a) where the two are sheared with respect to one another. (a) Vertical displacement. (b) Vertical displacement with rotation showing tilt. (c) Horizontal displacement. (d) Horizontal displacement with rotation showing tilt.

(1970), and Wasowski (1970). Moiré has also been used to compare an object to a master and for vibration analysis (Der Hovanesian and Yung 1971; Gasvik 1987). A theoretical review and experimental comparison of moiré and projection techniques for contouring is given by Benoit et al. (1975). Automatic computer fringe analysis of moiré patterns by finding fringe centers were reported by Yatagai et al. (1982). Heterodyne interferometry was first used with moiré fringes by Moore and Truax (1977), and phase measurement techniques were further developed by Perrin and Thomas (1979), Shagam (1980), and Reid

Classical Interferogram Analysis

- Elementary analysis of interferograms
- Computer analysis of interferograms

Typical Interferogram

Surface Error =
$(\lambda/2)\,(\Delta/S)$

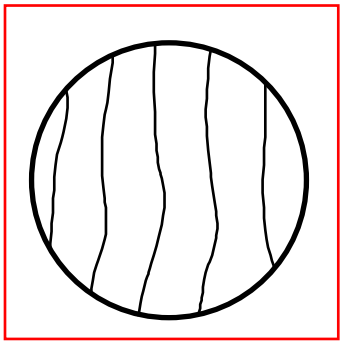

Classical Analysis

Measure positions of fringe centers.

Deviations from straightness and equal spacing gives aberration.

Elementary Interferogram Analysis

Estimate peak to valley (P-V) by looking at interferogram.

Dangerous to only estimate P-V because one bad point can make optics look worse than it actually is.

Better to use computer analysis to determine additional parameters such as root-mean-square (RMS).

Computer Analysis of Interferograms

Largest Problem

Getting interferogram data into computer

Solutions

- Graphics Tablet
- Scanner
- CCD Camera
- Phase-Shifting Interferometry

Automatic Interferogram Scanner

One solution

Video system and computer automatically finds locations of two sides of interference fringe where intensity reaches a given value.

Fringe center is average of two edge locations.

Digitization

Computer Analysis Categories

- Determination of what is wrong with optics being tested and what can be done to make the optics better.
- Determination of performance of optics if no improvement is made.

Minimum Capabilities of Interferogram Analysis Software

- RMS and P-V
- Removal of desired aberrations
- Average of many data sets
- 2-D and 3-D contour maps
- Slope maps
- Spot diagrams and encircled energy
- Diffraction calculations - PSF and MTF
- Analysis of synthetic wavefronts